Mesenchymal Stem Cell-derived Extracellular Vesicles with High PD-L1 Expression for Autoimmune Diseases Treatment

Fang Xu[1], Ziying Fei[1], Huaxing Dai[1], Jialu Xu[1], Qin Fan[1], Shufang Shen[1], Yue Zhang[1], Qingle Ma[1], Jiacheng Chu[1], Fei Peng[2], Fangfang Zhou[3], Zhuang Liu[1], Chao Wang[1]*

[1] Institute of Functional Nano & Soft Materials (FUNSOM), Jiangsu Key Laboratory for Carbon-based Functional Materials and Devices, Soochow University, Suzhou, Jiangsu 215123, China

[2] Wellman Center for Photomedicine, Massachusetts General Hospital, Harvard Medical School, Charlestown, MA 02114, USA

[3] Institutes of Biology and Medical Science, Soochow University, Suzhou 215123, China.

* Corresponding author: Chao Wang: cwang@suda.edu.cn;

Abstract

Autoimmune diseases are the third most common disease influencing the quality of life of many patients. Here, we develop a PD-L1+ mesenchymal stem cell (MSC) derived extracellular vesicles (MSC-sEVs-PD-L1) using lentivirus-mediated gene transfection technology for reconfiguration of the local immune microenvironment of affected tissue in autoimmune diseases. MSC-sEVs-PD-L1 exhibits an impressive ability to regulate various activated immune cells to an immunosuppressed state *in vitro*. More importantly, in dextran sulfate sodium (DSS)-induced ulcerative colitis (UC) and imiquimod-induced psoriasis mouse models, we observe a significantly high accumulation of MSC-sEVs-PD-L1 in the inflamed tissues compared to the PD-L1+ MSCs. Therapeutic efficiency in both UC and psoriasis mouse disease models is demonstrated using MSC-sEVs-PD-L1 to reshape the inflammatory ecosystem in the local immune context. We develop a technology using MSC-sEVs-PD-L1 as a natural delivery platform for autoimmune diseases treatment with high clinical potential.

This article has been accepted for publication and undergone full peer review but has not been through the copyediting, typesetting, pagination and proofreading process, which may lead to differences between this version and the Version of Record. Please cite this article as doi: 10.1002/adma.202106265.

Introduction

Our immune system not only defenses against pathogens, but also maintains homeostasis though immunosurveillance to control the inflammation due to environmental insults[1, 2]. Autoimmune disease is caused by the imbalance of the immune system that disturbs immunological tolerance[3, 4]. With the changes of living environment as a result of climate fluctuations and globalization, the global average annual rate of incidence and prevalence of autoimmune diseases have significantly increased by 19.1% and 12.5% over the past 30 years[5]. According to statistics, the autoimmune diseases have become the third largest chronic disease ranked after cardiovascular disease and cancer[3]. Meanwhile, the global autoimmune disease treatment drugs are in a steady growth trend with significant investment of time and money[6].

Pathological situations in auto-immunity can be characterized by inflammatory responses that do not resolve[3, 4]. Most patients need long-term or even lifelong medication, and some diseases (such as lupus nephropathy) are dangerous, seriously influencing the quality of life of patients. In addition to controlling the inducement, the clinical treatment for many autoimmune diseases mainly adopts the methods of inhibiting or blocking the pathological autoimmune response *in vivo*[7, 8]. Certain first-line drugs that majorly targeting interleukin-1 (IL-1), interleukin-6 (IL-6) and tumor necrosis factor-α (TNF-α) molecules have proven to be beneficial in clinical treatment[9, 10]. Although promising, the commonly used immunosuppressive drugs are usually non-specific. In addition, long-term use or high dosage of these drugs lead to drug resistance and adverse reactions, such as increasing risks of infection and malignancy[11]. Therefore, it is urgent to develop more efficient and targeted therapeutic strategies to calm down the unwanted inflammatory immune responses in the affected tissue in autoimmune diseases.

Immune responses are often regulated by immune checkpoint pathways, which plays pivotal roles in inducing and maintaining self-tolerance, preventing the immune system from attacking healthy tissue indiscriminately[12]. Among them, PD-1/PD-L1 signaling pathway is one of the important component in inhibiting the initial and effect stages of the immune responses and

maintaining the immune homeostasis[13]. Recent studies have shown that PD-1 or PD-L1 knockout can cause a variety of autoimmune diseases, such as systemic lupus erythematosus, rheumatoid arthritis, type 1 diabetes mellitus, *etc*[14, 15]. Enhancement of PD-1/PD-L1 interaction inhibits the proliferation and activation of antigen-specific T and B cells and the production of inflammatory cytokines to alleviate autoimmune encephalomyelitis and NOD diabetes in mice[16, 17]. Moreover, PD-1/PD-L1 inhibitors cause a series of collateral immune-related adverse reactions during cancer treatment, such as colitis, diabetes, hepatitis, arthritis[18, 19], indicating the important regulatory role of PD-1/PD-L1 signaling pathway in maintaining immune system balance.

Mesenchymal stem cells (MSCs) therapy is a cell-based treatment for inflammatory disorders. MSCs have great immunosuppressive properties which can inhibit T cell activation and alter the phenotype of macrophages and dendritic cells in various pre-clinical and clinical studies[20]. However, the safety of MSCs is still under debate. Moreover, the preparation of homologous MSCs is costly and time-consuming with several limitations such as storage problem and cell senescence during expansion. Thus, their clinical use is challenging and easy to form pulmonary embolism following the intravenous administration[21]. Compared to MSCs, MSC derived extracellular vesicels (MSC-sEVs) feature not only the similar immunoregulatory capacity but also the advantages including low immunogenicity and high plasticity[22]. In this work, a high-expressing PD-L1 extracellular vesicles derived from lentivirus-mediated gene transfection MSC (MSC-sEVs-PD-L1) were prepared for various autoimmune diseases treatment. Interestingly, the great targeting ability of MSC-sEVs-PD-L1, but not MSC-PD-L1, was found in DSS-induced colitis mice. Furthermore, MSC-sEVs-PD-L1 significantly restored tissue lesion by reshaping the local immune microenvironment. Our results indicated that the MSC-sEVs-PD-L1 might potentially provide a universal platform technique for the immunotherapy of various autoimmune diseases.

Results

Enhancement of PD-1 expression in autoimmune pathological tissue

PD-1 is an important inhibitory receptor, which plays a pivotal role in the maintenance of self-tolerance. It is primarily expressed on various activated immune cells (including T cells, B cells, macrophages, and DCs *etc*.)[13]. When interacting with its ligands, PD-L1 and PD-L2, these activated immune cells result in the state of exhaustion, dysfunction and increased apoptosis, thereby limiting the function of detrimental hyperinflammatory responses during chronic infection and auto-immunity[23]. Firstly, we confirmed the correlation of PD-1 expression in the inflamed tissue in the context of many autoimmune diseases. GEO (Gene Expression Omnibus) data analysis of patients' tissue sample including ulcerative colitis (UC), psoriasis and rheumatoid arthritis (RA) as well as in peripheral blood mononuclear cells of juvenile rheumatoid arthritis, diabetic children, and lupus erythematosus patients correlated with a higher expression of PD-1 gene compared to that in healthy samples (**Fig. 1, A to F**). To further explore their correlation, we established preclinical models including DSS-induced mouse UC and IMQ-induced mouse psoriasis. Immunohistochemistry results also demonstrated a significantly high PD-1 expression in the inflamed colon and skin tissues (**Fig. 1, G and H**). The quantification data including flow cytometry analysis and qPCR results suggested the upregulation of PD-1 expression in inflammation tissue compared to normal group (**Fig. 1, I to L**). The expression of PD-1 indicated the activation of various immune cells that may contribute to continuous development of inflammation.

Characterization of MSC-sEVs-PD-L1

Bone marrow derived MSCs were obtained from C57BL/6 mice. The morphology of MSCs was observed by microscope and analyzed by flow cytometry. As shown in **Fig. S1**, the MSCs were displayed spindle-shaped or irregular triangular-shaped under microscope (**Fig. S1A**). The purity of MSCs was assessed by marker expression with CD105, CD73, CD90 positively, and CD34, CD45 negatively (**Fig. S1, B and C**). MSCs derived extracellular vesicles (MSC-sEVs) as a cell-free vesicle has been demonstrated alternative therapies for a variety of

inflammatory diseases, due to their potential to regulate immune response. As shown in **Fig. 2A**, to generate PD-L1 overexpression MSC-derived extracellular vesicels (MSC-sEVs-PD-L1), PD-L1$^+$ MSCs were established by infection with lentivirus and puromycin screening. PD-L1 was expressed and localized on the cell membrane indicated by the co-localization of GFP-PD-L1, the cell membrane dye Alexa Fluor 594-conjugated wheat germ agglutinin (WGA594), and MSC marker CD44 fluorescence signal (**Fig. 2B**). PD-L1 expression was further confirmed by flow cytometry (**Fig. 2C**), indicating a high PD-L1 expression on MSCs. The MSC-derived extracellular vesicles were then isolated and purified according to an established protocol[24]. Transmission electron microscopy (TEM) imaging showed spherical morphology of MSC-sEVs (**Fig. 2D**) with an average diameter around 100 nm (**Fig. 2E**), which had no significant difference compared to MSC-sEVs-PD-L1. They contained extracellular vesicles-associated proteins, *e.g.*, CD63, CD9 and MSCs specific marker CD73 (**Fig. 2F**). Furthermore, we identified the existence of high level of PD-L1 on MSC-sEVs-PD-L1 (**Fig. 2F**). These results showed that we successfully prepared PD-L1 overexpressed MSC-derived extracellular vesicles.

MSC-sEVs-PD-L1 effectively inhibited immune cells activation *in vitro*

To study the immunomodulation potential of MSC-sEVs-PD-L1, we evaluated whether it could effectively calm down overactivated immune cells *in vitro*. In our experiment, activated BMDM cells and BMDCs induced by LPS, or activated lymph node T cells induced by anti-CD3/CD28, were incubated with sEVs-PD-L1 for 24 h. The immunofluorescence imaging showed the remarkable co-localization of sEVs-GFP-PD-L1 and PD-1, suggesting their interaction which was blocked by PD-L1 antibody (**Fig. 3A and Fig. S2**). To study the immunoregulatory role of MSC-sEVs-PD-L1 to these immune cells, flow cytometric analysis was used to assess the functional orientation of each cellular component *in vitro*. It was observed that anti-CD3/CD28 treatment induced IFN-γ production by CD4+ T cells, while MSC-sEVs-PD-L1 remarkably reduced the CD4+ IFN-γ+ frequency (**Fig. 3, B and C**). At the same time, we further found that MSC-sEVs-PD-L1 increased Foxp3 expression and enhanced the population of Tregs, which are crucial in suppressing immune response and maintaining

self-tolerance (**Fig. 3D**). We also detected a decrease in Ki-67+ CD3+ T cells (**Fig. 3E**) and a promoted CD3+ T cells apoptosis (**Fig. 3F**) following MSC-sEVs-PD-L1 treatment. As a result, MSC-sEVs-PD-L1 resulted in T cells anergy, regularly T cell induction and effector T cell elimination.

In addition to T cells, LPS-activated BMDM cells or BMDCs were incubated with MSC-sEVs-PD-L1 for analysis. The expression of CD80, one of the pro-inflammatory phenotype (M1-like) markers on macrophages, was drastically declined after MSC-sEVs-PD-L1 treatment. While the frequency of anti-inflammatory CD206+ macrophage (M2-like) was increased following the treatment (**Fig. 3G**). For BMDCs, LPS dramatically induced the maturation of DCs, indicated by the high level of CD80 and CD86 costimulatory molecules expression. In contrast, MSC-sEVs-PD-L1 significantly lowered the CD80/CD86 level, indicating the inhibitory effect of MSC-sEVs-PD-L1 to BMDCs (**Fig. 3H**). Meanwhile, we measured the content of cytokines released from immune cells in the medium (**Fig. 3I**). MSC-sEVs-PD-L1 decreased inflammatory cytokines (IL-1β, TNF-α) production and elevated the IL-10 release from LPS-induced BMDM cells. In medium of lymph node cells, MSC-sEVs-PD-L1 blocked the production of IFN-γ and IL-2, and enhanced IL-4 expression. The observed suppressive effects on multiple immune cells activation was blocked by PD-L1 antibody treatment. Taken together, these results showed that MSC-sEVs-PD-L1 altered the phenotype of various activated immune cells to immunosuppressed state and inhibited inflammatory cytokines production.

MSC-sEVs-PD-L1 therapy for DSS-induced ulcerative colitis

Ulcerative colitis (UC) is an autoimmune disease accompanied with hematochezia, diarrhea, weight loss and severe inflammation, and has no effective treatment so far[25]. To explore the *in vivo* UC inhibition efficiency of MSC-sEVs-PD-L1, we firstly analyzed their distribution in tissues of healthy and DSS-induced colitis mice following the intravenous injection. Interestingly, Caliper IVIS Lumina II *ex vivo* imaging and immunofluorescence results showed

that DiD-labelled MSC-sEVs-PD-L1 remarkably gathered in the colon of DSS-induced colitis mice (**Fig. 4, A and B**) and remained for 24 h after intravenously injection (**Fig. S3**). Conversely, MSCs-PD-L1 displayed an obvious retention in lung and feeble accumulation capacity to colon under the same condition (**Fig. S4, A and B**). In addition, we compared the therapeutic efficiency of MSC-PD-L1 and MSC-sEVs-PD-L1 in DSS-induced colitis mice. The results showed that MSC-PD-L1 played a negligible role in the treatment compared to MSC-sEVs-PD-L1 (**Fig. S4, C to E**). Moreover, in DSS-induced colitis, the signal of MSC-sEVs-PD-L1 was found in T cells (CD3+), macrophages (F4/80+) and DCs (CD11c+) of colon tissue assessed by flow cytometry (**Fig. 4C**).

To determine whether MSC-sEVs-PD-L1 relieved the UC, DSS-challenged mice were intravenously injected PBS, MSC-sEVs, MSC-sEVs-PD-L1 or MSC-sEVs-PD-L1+Anti PD-L1 over 7 days (daily dose = 50 μg per mice) (**Fig. 4D**). Interestingly, we observed that mice received MSC-sEVs-PD-L1 significantly rescued the weight loss as compared to mice treated with PBS or MSC-sEVs (**Fig. 4E**). The therapeutic efficiency of MSC-sEVs-PD-L1 was also associated with reduced disease activity index (**Fig. 4F**) and shorten the colon (**Fig. 4, G and H**) relative to controls. Histological analysis further confirmed the effectiveness of MSC-sEVs-PD-L1, which relieved distortion of crypts, loss of goblet cells, infiltration of inflammatory cells, severe mucosal damage (**Fig. 4I**) and mucosa tight junction protein Claudin-1 reduction (**Fig. 4J**). In addition, MSC-sEVs-PD-L1 significantly improved intestinal tissue permeability in DSS challenged mice (**Fig. 4K**). In line with *in vitro* result, the restored tissue lesion was blocked by PD-L1 antibody treatment. These results clearly revealed that MSC-sEVs-PD-L1 ameliorated DSS-induced ulcerative colitis.

To define the mechanisms of MSC-sEVs-PD-L1 for UC relief, we then characterized the colon ecosystem in mice at day 8. Immunohistochemistry of colon showed that MSC-sEVs-PD-L1 dramatically diminished the infiltration of CD45, CD11c, F4/80, CD4 T cells in colon of DSS

challenged mice (**Fig. 5A**). Then the frequency and activation of various immune components were investigated by flow cytometry analysis. In line with the immunohistochemistry results, a significant reduction of CD45+ cells (**Fig. 5B**) and inhibition of DCs (**Fig. 5, C and D**) and macrophages (**Fig. 5, E to G**) were observed. In addition, there was a significant reduction in CD3+ and CD4+ T cells abundance (**Fig. 5, H to J**), and the remarkable elevation in Treg (Foxp3+) population in the colon tissue as a consequence of MSC-sEVs-PD-L1 treatment compared to controls (**Fig. 5K**). Furthermore, we detected IFN-γ, IL-17a or IL-4 producing T cells in mice after various treatments. There was a considerable decrease in the percentage and absolute number of IFN-γ+CD4+ and IL-17a+CD3+ cells in MSC-sEVs-PD-L1-treated mice compared with control mice (**Fig. 5, L and M**). In contrast, IL-4 producing CD4+ T cells were induced following the MSC-sEVs-PD-L1 administration (**Fig. 5N**). These results suggested that the MSC-sEVs-PD-L1 might inhibit the proliferation of T cells and regulate Th1, Th2, Th17, and Treg cells responses in colon of DSS-induced acute colitis mice. Immune cells populations of peripheral blood were also determined and results showed that MSC-sEVs-PD-L1 decreased Th1, Th17, monocytes cells distribution and increased Th2 cells responses (**Fig. S5**). Measurement of cytokine mRNA relative levels including *Il-17a*, *Ifn-γ*, *Il-6*, *Tnf-α*, *Il-1β* and *Il-4* in colon tissues showed that MSC-sEVs-PD-L1 reduced pro-inflammatory cytokines expression, and enhanced anti-inflammatory cytokines generation (**Fig. 5O**), which in accordance with colonic and serum cytokines (**Fig. S6**). While the capacity of immune response regulation of MSC-sEVs-PD-L1 was disturbed by PD-L1 antibody. Taken together, these results suggested that the therapeutic effect of MSC-sEVs-PD-L1 was resulted from their ability to reshape the inflammatory ecosystem in colon of colitis mice by manipulating and regulating the local and systemic immune context.

MSC-sEVs-PD-L1 therapy for IMQ-induced psoriasis

We next questioned whether MSC-sEVs-PD-L1 could be broadly applicable for other autoimmune disease. Psoriasis as a common autoimmune disease is characterized by red-colored plaques, skin lesions covered by slivery-white dry scales and inflammatory thickness[26]. Caliper IVIS Lumina II *ex vivo* imaging displayed the abundant accumulation of

DiD-labelled MSC-sEVs-PD-L1 in skin of mice treated with imiquimod (**Fig. 6A**). We assessed the therapeutic effect of MSC-sEVs-PD-L1 on a preclinical model of psoriasis induced by imiquimod (IMQ) (**Fig. 6B**). IMQ-treated mice continuously increased clinical scores with weight loss. Encouragingly, we again observed that MSC-sEVs-PD-L1 administration significantly alleviated these symptoms (**Fig. 6, C and D**). Both skin and epidermal thickness were obviously reduced in mice receiving MSC-sEVs-PD-L1 compared with controls (**Fig. 6, E and F**). The level of red-colored plaques and slivery-white dry scales on skin induced by IMQ were also alleviated by MSC-sEVs-PD-L1 treatment (**Fig. 6G**). Besides, histopathological assay of skin sections further supported the therapeutic efficiency of MSC-sEVs-PD-L1 (**Fig. 6H**), which inhibited acanthosis, parakeratosis, and thickening of the stratum corneum remarkably. Dilatation of blood vessels and immune cells infiltration in the dermis was reduced in the treatment group compared with controls. Immunohistochemical and flow cytometry analysis were used to further characterize the local ecosystem following the treatment. Immunohistochemistry staining showed a significant reduced immune cells infiltration in the affected skin tissue following the MSC-sEVs-PD-L1 treatment (**Fig. 6I**). Quantification of various immune cell components by flow cytometry demonstrated that MSC-sEVs-PD-L1 significantly suppressed the inflammatory response by reduction of immune cells infiltration, alteration of their phenotype (**Fig. 6, J to R**), activation of immunoregulatory cells (**Fig. 6S**) and regulation of inflammatory/ immunoregulatory cytokines in skin and perpherial circulation (**Fig. 6, T to V, Fig. S7, Fig. S8**), which was broken by PD-L1 antibody treatment. Collectively, these results confirmed that our strategy can provide a broaden platform for autoimmune diseases therapy.

Safety evaluation of MSC-sEVs-PD-L1 *in vivo*

As cell-derived biological nanoparticles with high complexity, we next evaluated the safety of MSC-sEVs-PD-L1 *in vivo*. As shown in H&E staining, MSC-sEVs-PD-L1 treatment in healthy mice had no effect on tissue structure, cellular morphology and immune cells infiltration (**Fig. 7A**). The proportion of immune cells in major tissue was further analyzed by flow cytometry. It was showed that MSC-sEVs-PD-L1 could slightly affect the macrophages

population in liver but did not distinctly influence other immune context of major tissues (**Fig. 7B**). In addition, liver and kidney functional indicators (ALT, AST, CREA, UA) and the level of HGB, lymphocytes, monocytes, neutrophils, PLT, RBC, WBC of blood showed no markedly difference compared to PBS group (**Fig. 7, C and D**). Taken together, the MSC-sEVs-PD-L1 exhibited great biocompatibility to mice.

Discussion

Immune checkpoints act as a critical molecule in maintaining the stability of immune system. Accumulating clinical data suggested that PD-1/PD-L1 plays an important role in a variety of autoimmune diseases. Targeting PD-1/PD-L1 has been successfully demonstrated in treating cancers[27]. It has also been considered as a promising strategy to target this pathway in autoimmune and inflammatory disorders.

Recent years, researchers have developed several biological vectors with high PD-L1 expression for autoimmune disease treatment. For example, genetically modified platelet with PD-L1 overexpression could efficiently inhibit the activity of autoreactive T cells, protect β cells from attacking in type 1 diabetic NOD mice[28]. Similarly, overexpression of PD-L1 on hematopoietic stem cells and progenitor cells also had the therapeutic effect for reversing diabetes in newly hyperglycemic NOD mice[17]. Besides, IFN-γ induced PD-L1+ MSCs have shown to regulate T cell-mediated immunosuppression, increase the proportion of regulatory T cells, and maintain peripheral immune tolerance[29]. Although the above cellular vectors with high PD-L1 expression played an effective role in the treatment of autoimmune diseases, the targeting ability to the pathological tissues remains challenging due to their micro-size, which is easy to form pulmonary embolism following the intravenous administration (**Fig. S3A**). In addition, the preparation of live cells is also very costly and time-consuming with several limitations such as cell senescence, storage problems, and so forth. Studies have reported the beneficial effects of non-engineered sEVs on autoimmune diseases, nervous system disease, cardiovascular diseases treatment[30-32]. In our study, the dosage of sEVs was 50 μg per mice

that lower than the previous reports (>100 μg), which could explain the limited effect on therapeutic efficiency of non-engineered sEVs in our results. Together we indicated that PD-L1 expression could enhance the efficacy of non-engineered sEVs on autoimmune diseases treatment.

In this work, we constructed a targeted therapeutic strategy using nano-sized MSC-sEVs-PD-L1 to target PD-1, which is highly expressed in autoimmune pathological tissues. The great targeting ability of MSC-sEVs-PD-L1, but not MSC-PD-L1, was confirmed in DSS-induced colitis mice (**Fig. 4, A and B, Fig. S3, A and B**). The underlying causes likely include (i) chemotaxis of MSC-sEVs. The extracellular vesicles derived from MSC expresses a wide range of chemokine receptors that in response to chemokines produced in inflammatory site[33]; (ii) nano-size of MSC-sEVs. The increase in vascular permeability in inflamed tissue allows more fluid, macromolecules, as well as extracellular vesicles to reach the affected tissue by passing out of the small blood vessels[34]. In addition, *in vivo* data showed that MSC-sEVs-PD-L1 could be recognized by various activated immune cells including T cells (CD3+), macrophages (F4/80+) and DCs (CD11c+) with high PD-1 expression (**Fig. 4C**), facilitating the PD-1 and PD-L1 interaction in the inflammatory conditions.

Autoimmune diseases can cause systemic inflammation. Inflammatory factors released by the activation of immune cells enter the blood circulation system and activate immune cells, causing uncontrollable inflammatory damage to other normal tissues and organs, such as lupus nephritis and psoriatic arthritis[35, 36]. Also, in DSS-induced ulcerative colitis and imiquimod-induced psoriasis, we found a significant increase of immune cells (*e.g.*, Th1/Th17 cells) and pro-immflammatory cytokines at both local and peripheral criculation. Enhanced therapeutic efficiency was observed following the MSC-sEVs-PD-L1 administration. The abundance and functional orientation of each cellular component and cytokines expression of the autoimmune pathological microenvironment and systemic levels was investigated following the treatment. We found that MSC-sEVs-PD-L1 inhibited the proliferation of T

cells, DCs and macrophages. CD4+ T-helper cells play crucial roles in the various autoimmune diseases[37]. We further found that MSC-sEVs-PD-L1 regulated Th1, Th2, Th17, and Treg cells responses and balanced in Th subtype. IFN-γ+CD4+ and IL-17a+CD3+ T cells were decreased while IL-4+ and Foxp3+ CD4+ T cells were increased. The cytokine expression and mRNA relative levels including *Il-17a*, *Ifn-γ*, *Il-6*, *Tnf-α*, *Il-1β* and *Il-4* in colon tissues also confirmed our results. In peripheral circulation, immune cell populations and cytokines expression were in consistent with local organs modulated by MSC-sEVs-PD-L1. Taken together, MSC-sEVs-PD-L1 resulted in reconfiguration of local immune microenvironment by regularly T cells induction and effector T cells elimination and associated cytokines expression modulation. In addition, MSC-sEVs-PD-L1 alleviated systemic inflammatory response by inducing immune cells inactivation in cirulation. Lastly, side effects were limited and the mice were well tolerated following the treatment. However, the long-term side effects still need to be investigated before the clinical translation.

In conclusion, we developed PD-L1 overexpressed MSC-derived extracellular vesicles as cell-free carrier for treatment of autoimmune diseases. We demonstrated that MSC-sEVs-PD-L1 significantly targeted and restored tissue lesion by inhibition the inflammatory immune cells via PD-1/PD-L1 pathway. Our MSC-sEVs-PD-L1 technology may have promising clinical translation potential due to its ease of preparation, low-cost, feasibility and biosafety.

Materials and methods

Regents

DSS (Dextran sulfate sodium, 9011-18-1), LPS (Lipopolysaccharide, L2630), GM-CSF (SRP3201), IL-4 (SRP3211), M-CSF (SRP3221), and FITC-dextran (4 kD, 46944) were purchased from Sigma-Aldrich (St. Louis, Missouri, USA). Aldara (5 % imiquimod cream) was obtained from 3M Health Care Limited. Anti-mouse CD3 (100202) and anti-mouse CD28 (16-0281038) were respectively purchased from BioLegend and eBioscience. GFP-PD-L1 lentivirus was manufactured by HanBio Company (Shanghai, China). Annexin V-FITC /

propidium iodide assay kit (C1062S) for flow cytometry was purchased from Beyotime Biotechnology (Shanghai, China). Elisa kit for murine IL-1β (EM2IL1B), IL-6 (BMS603-2), TNF-α (BMS607-3), IL-4 (BMS613), IL-10 (88-7105-22) were purchased from Invitrogen (Carlsbad, CA), IFN-γ (430807), IL-2 (431007), IL-17a (432507) were purchased from Biolegend (San Diego, CA). DiD labeling solution (V22887), 40, 6-diamidino-2-phenylindole (DAPI, D3571) was purchased from Invitrogen (Carlsbad, CA). Antibodies for Western blot, flow cytometry and immunohistochemistry used in this study were described in Supporting Table 1.

Animals

C57BL/6 mice (female, 6-8 weeks old, 18-22 g) were purchased from the experimental animal center of Soochow University. They were maintained with free access to pellet food and water in plastic cages 21±2°C and kept on a 12 h light/dark cycle in specific pathogen-free facilities. Animal welfare and experimental procedures were carried out strictly in accordance with Institutional Review Board of Soochow University. And all efforts were made to decrease animals' suffering and to reduce the number of animals used in this manuscript.

Cell culture

6-8 weeks old C57BL/6 mice were euthanized to isolate bone marrow cells according to an established method[38]. In brief, C57BL/6 mice were euthanized and femurs were dissected using a 21-ga needle flushed femurs with PBS. After centrifugation at 300 *g* for 5 min at 4 °C, cells were grown in RPMI 1640 (GIBCO, Grand Island, NY) medium containing 10 % fetal bovine serum and 20 ng/mL GM-CSF, 20 ng/mL IL-4 to differentiate into bone marrow-derived dendritic cells (BMDCs)[39] or 20 ng/mL M-CSF to differentiate into bone marrow-derived macrophage cells (BMDM)[40] in 5 % CO_2 at 37 °C for 7 days. For M1 macrophage polarization and BMDCs maturity, BMDM cells and BMDCs were treated with 50 ng/mL LPS for 24 h.

Lymph node cells of inguinal were obtained from C57BL/6 mice, and grown in RPMI 1640 (GIBCO, Grand Island, NY) medium containing 10 % fetal bovine serum and 2 μg/mL anti-CD3 and 5 μg/mL anti-CD28 in 5 % CO_2 at 37 °C for 48 h.

Mesenchymal stem cells were isolated from C57BL/6 mice mouse bone marrow according to an established method[41, 42]. C57BL/6 mice were euthanized and femurs were dissected, using a 21-ga needle flushed femurs with PBS. After centrifugation at 300 *g* for 5 min at 4 °C, and bone marrow cells were seeded in 60 mm^2 culture plates at a density of 4×10^6 in basic DMEM (GIBCO, Grand Island, NY) medium containing 10 % fetal bovine serum and 100 U/mL penicillin, and 100 mg/mL streptomycin in 5 % CO2 at 37 °C. After 12 h, removed nonadherent cells and replaced with fresh medium. Thereafter, the medium was refreshed every 3 days and continuous culture until the purity of mesenchymal stem cells reached 80 %-90 %. The purity of isolated MSCs was determined by flow cytometry using MSCs specific markers of CD34-, CD45-, CD105+, CD73+, CD90+.

Extraction and purification of mesenchymal stem cell derived extracellular vesicles with PD-L1 overexpression (MSC-sEVs-PD-L1).

Mesenchymal stem cell was performed lentivirus transfection experiment to overexpress PD-L1 with 7 μg/mL purinomycin screening. When the transfection efficiency reached 70-80 % measured by Western blot and flow cytometry analysis. The EVs in medium and FBS were depleted by ultracentrifugation[43]. The medium was replaced by an EV-depleted medium and collected after 48 h. MSC-sEVs were isolated and purified by ultracentrifugation. In brief, the medium was centrifuged at 300 *g* for 10 min, 1000 *g* for 10 min, 2000 *g* for 10 min, 10000 *g* for 30 min, 100000 *g* for 70 min at 4 °C, to obtain mesenchymal stem cell derived extracellular

vesicles. MSC-sEVs specific marker expression of CD63, CD9, CD73 and the PD-L1 expression was measured by Western blot.

Transmission electron microscopy (TEM)

Freshed MSC-sEVs sample was pipetted onto a 300 mesh copper and incubated for 3 min. Then, removed excess liquid and washed twice with distilled water. 20 μl of 1 % uranyl acetate was pipetted onto the mesh copper and incubated for 1 min, washed with distilled water and placed in a clean dish to dry for transmission electron microscopy. The images were acquired using a FEI TF20 transmission electron microscopy at 200 kV.

MSC-sEVs size determination by dynamic light scattering (DLS).

The volume of MSC-sEVs and MSC-sEVs-PD-L1 sample was increased to 1 ml by PBS and loaded into a quartz cuvette. The size distribution of sEVs was measured by dynamic light scattering at 25 ℃ and analyzed using FLEX software.

Animal model induction and treatment

Mice were randomly assigned into five experimental groups and used after acclimating to the housing environment for 7 days: (1) Normal, (2) model, (3) MSC-sEVs, (4) MSC-sEVs-PD-L1, (5) MSC-sEVs-PD-L1+Anti PD-L1. 50 μg MSC-sEVs-PD-L1 were inocubated with 50 μg PD-L1 antibody *in vitro* for 2 h, and washed three times with PBS by ultracentrifugation. Mice were intravenously injected with MSC-sEVs,,MSC-sEVs-PD-L1 and MSC-sEVs-PD-L1+Anti PD-L1 (daily dose = 50 μg per mice) once a day. Data collection and analysis were performed blindly. The experimenters were unaware of the group assignment and animal treatment.

Ulcerative colitis as an autoimmune disease was induced by adding 3 % dextran sulfate sodium (DSS) in drinking water for 7 days[44], and mice were treated with MSC-sEVs, MSC-sEVs-PD-L1 and MSC-sEVs-PD-L1+Anti PD-L1 intravenously (*i.v.*) administration, except for mice in normal and ulcerative colitis group. Body weight, stool consistency, and the presence of gross blood in feces and at the anus were recorded every day. The disease activity index was calculated by assigning well-established and validated scores as previously described[45]. Generally, a) diarrhea (0 point = normal, 2 point = loose stool, 4 point = watery diarrhea), b) hematochezia (0 point = no bleeding, 2 point = slight bleeding, 4 point = gross bleeding), the disease activity index scores were summed up with a) and b).

Psoriasis was induced by applying mice with Aldara imiquimod (IMQ) cream[46] (3M Health Care, Leicestershire, UK) topically daily on shaved skin for 4 constitutive days (daily dose = 62.5 mg per mice), and mice were treated with MSC-sEVs, MSC-sEVs-PD-L1 and MSC-sEVs-PD-L1+Anti PD-L1 intravenously (*i.v.*) administration, except for mice in normal and psoriasis group. The severity of disease was measured with the adapted human clinical Psoriasis Area and Severity Index[47], which was cumulated with three clinical signs (erythema, induration and desquamation) on a scale from 0 to 4: 0, none; 1, slight; 2, moderate; 3, marked; and 4, very marked. Mice were scored daily, and body weight was monitored. Mice were sacrificed on day 4 when the score reached a plateau. Back skin was obtained, and the thickness was measured with a digimatic micrometer (0.001 mm; Mitutoyo Company, Tokyo, Japan). Then, the skin samples were cut into several parts for the following detections.

Flow cytometry analysis

Cultured cells were harvested or separated from tissues crushed by tissue grinding to obtain a single-cell suspension and treated with red blood cell lysis buffer, then washed with cold PBS two times, and stained with a combination of fluorescence-conjugated mouse mAbs as listed in

Supporting Table 1. For surface staining, cells were inocubated with antibodies of PE-CD45, FITC-CD3, APC-CD4, FITC-CD11c, FITC-F4/80, PE-CD80, APC-CD206, APC-CD86, APC-CD14, FITC-CD16, APC-CD34, APC-CD105, FITC-CD73, APC-CD90.2 for 30 min in the dark at room temperature. For intracellular staining, cells were fixed in 4 % paraformaldehyde (PFA) for 30 min at room temperature. After being washed with Perm/Wash buffer, cells were inocubated with antibodies of PE-Foxp3, PE-IFNγ, APC-IL-17a, APC-IL-4, Percp-Ki67 for 30 min in the dark at room temperature. The cells apoptosis was analyzed by staining with Annexin Ⅴ / PI for 30 min in dark at room temperature. Then all samples were washed three times with cold PBS, and analyzed by BD Accuri C6 flow cytometer and FlowJo.

Intestinal tissue permeability analysis

Colon barrier function was evaluated using the permeability tracer fluorescein isothiocyanate (FITC)-labelled dextran[25]. Mice of 6-8 weeks old were challenged with 3 % DSS and treated with MSC-sEVs,,MSC-sEVs-PD-L1 and MSC-sEVs-PD-L1+Anti PD-L1 intravenously (*i.v.*) for 7 days. Mice were gavaged with 0.6 mg/g body weight of a 60 mg/mL solution of FITC-dextran (4 KD) and serum was collected after 4 h. Fluorescence emission was measured at an excitation of 490 nm and an emission of 530 nm.

Western blot analysis

Western blot was performed according to the previous description[48]. Cells were collected and lysed by lysis buffer. The obtained protein lysates were quantitated by BCA assay, and degenerated at 100 °C for 5 min. Then, the proteins were separated by 10 % SDS-PAGE and electrophoretically transferred onto poiyvinylidene fluoride (PVDF) membranes (Millipore Corp, Bedford, MA). After that, the membranes were blocked with 3 % BSA for 1 h at room temperature, and incubated with specific primary antibodies overnight at 4 °C. Subsequently, the primary antibody-incubated membranes were washed 5 times with washing buffer before HRP-coupled secondary antibody labeling. Protein bands were visualized by Western blot

detection system according to the manufacturer's instructions (Cell Signaling Technology, MA).

Cytokine analysis by Elisa

Cytokines released to culture supernatant or serum were measured by Elisa kits according to the manufacturer's instructions. In brief, serum of each group was collected from peripheral blood by centrifuging at 1500 g for 10 min at room temperature, or each group culture supernatant of BMDM cells and lymph node T cells was collected. 100 μl /well of serum or supernatant samples was added to the plate with capture antibody and incubated at room temperature for 2 h or overnight at 4 ℃, and washed 3 times with 250 μl/well wash buffer. Blot plate on absorbent paper to remove any residual buffer. Added 100 μl/well diluted detection antibody to all wells and incubated at roo, temperature for 1 h, washed 3 times with 250 μl/well wash buffer. Added 100 μl/well of diluted avidin-HRP and inocubated at room temperature for 30 min, washed 3 times with 250 μl/well wash buffer. Added 100 μl /well of 1×TMB solution and incubated at room temperature for 15 min.Added 100 μl /well of stop solution and read plate at 450 nm and analyzed data.

Quantitative PCR

Total RNA was extracted from cells or tissues by Trizol. 1 μg mRNA was reverse-transcribed to cDNA and subjected to quantitative PCR, which was performed with the BioRad CFX96 ouchTM Real-Time PCR Detection System (Biorad, CA) using iQTM SYBR Green supermix (BioRad, CA). Threshold cycle numbers were obtained using BioRad CFX manager software. The program for amplification was 1 cycle of 95 °C for 2 min followed by 40 cycles of 95 °C for 10 s, 60 °C for 30 s, and 72 °C for 30 s. The primer sequences used in this study were shown in Supplementary Table 2. The relative expression of each gene was normalized to the expression of β-actin, and then reported as fold change of basal level.

Immunohistochemistry and histopathology analysis

Colon and skin samples were fixed in 10 % formalin solution (v/v) overnight at room temperature and prepared paraffin sections for hematoxylin and eosin (H&E), immunohistochemistry and immunofluorescence. Disease severity was determined by histopathological scoring of tissue H&E staining in a blinded fashion. Histopathological scoring of colon tissue is characterized by the combination of inflammatory cell infiltration and epithelial damage of colon[49]. Scores for inflammatory cell infiltration were summed by the mucosa (0, normal; 1, mild; 2, modest; 3, severe), submucosa (0, normal; 1, mild to modest; 2, severe) and muscle/serosa (o, normal; 1, modest to severe). The scores of epithelial damage were assigned as follows: 0, no epithelial damage; 1, hyperproliferation of the mucosa; 2, mild to moderate goblet cell loss (10 %-50 %); 3, severe goblet cell loss (50 %-90 %); 4, 100 % goblet cell loss; 5, presence of ulcer.

Immunohistochemistry

Paraffin-embedded tissues were heat-fixed, deparaffinized, rehydrated, antigen retrieval and subsequent process followed according to the manufacturer' instructions. First, tissue sections were heat-fixed for 2 h at 60 ℃ and deparaffinized in xylene for 30 min, then rehydrated in 100 %, 75 %, 50 % ethanol respectively for 10 min and washed with double-distilled water for 5 min. Antigen retrieval was performed by 10 mM citrate antigen retrieval solution under high pressure for 2 min. The sections was inocubated with 3 % H_2O_2 for 10 min in the dark, blocked by 3 % goat serum for 1 h and stained with CD45, CD11c, F4/80, CD4, PD-1, Claudin-1 overnight at 4 ℃, washed 3 times with PBST. 50 μl HRP-labelled goat anti-mouse/rabbit Ig mixture was added to sections for 30 min and washed with PBST for 3 times. 50 μl DAB reagent was added for color reaction and restained with hematoxylin for 30 s. Finally, the sections was soaked in 50 %, 75 %, 100 % ethanol and xylene for 10 min respectively to dehydrate. The images of samples were acquired by Leica fluorescence optical microscope.

Immunofluorescent microscopy

BMDM cells, BMDCs and lymph node cells were activated, and pretreated with DiD-labelled MSC-sEVs-PD-L1 for 24 h. Then cells fixed in 4 % paraformaldehyde (PFA) for 10 min at 37 °C, blocked with 3 % BSA for 1 h at room temperature, and stained with PD-1, CD3 antibody overnight at 4 °C. Then, the cells were washed three times with cold PBS, and stained with DAPI for confocal laser scanning microscope (Olympus Lake Success, NY) imaging.

Statistical analysis

All experiments were randomized and blinded. All studies were performed at least three independent experiments with each experiment including triplicate sets *in vitro*, or six animals per group *in vivo*. All data were presented as the mean ± SEM. GraphPad Prism 8.0 software (San Diego, CA, USA) was used for data statistical analysis. Shapiro-Wilk test and Kolmogorov-Smirnov test was used to calculate the normality of the data distribution. Because the data have passed normality test, Student's t-test was used to test the difference between two groups. $*P < 0.05$ was considered to be statistically significant.

Acknowledgment

This work was supported by National Natural Science Foundation of China (No. 32022043), the Natural Science Foundation of Jiangsu Province (No. SBK2019040088), Jiangsu Province Six Talent Peaks Project (No. SWYY-110). This work was also supported by the Program for Jiangsu Specially-Appointed Professors to C. W. This work was partly supported by Collaborative Innovation Center of Suzhou Nano Science & Technology, the Priority Academic Program Development of Jiangsu Higher Education Institutions (PAPD), the 111 Project.

Author contributions

C. W. and F. X. designed the project. F. X. performed the experiments, collected the data, and analyzed and interpreted the data. All authors contributed to the writing of the manuscript, discussed the results and implications, and edited the manuscript at all stages.

Competing interests

The authors declare no competing interests.

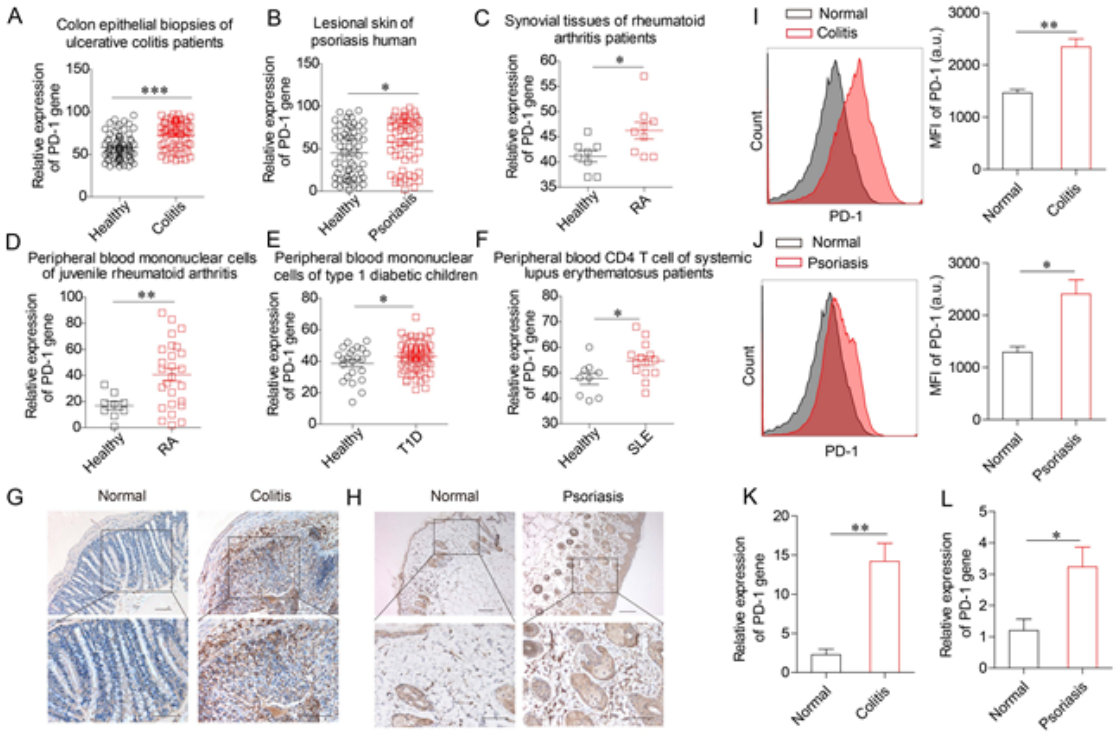

Fig. 1. Enhancement of PD-1 expression in inflamed tissue. (A-F) GEO data analysis of PD-1 gene expression in colon epithelial biopsies of ulcerative colitis patients (ID: 53092473), lesional skin of psoriasis patients (ID: 100689276), synovial tissues of rheumatoid arthritis patients (ID: 124856255) and peripheral blood mononuclear cells of juvenile rheumatoid arthritis (ID: 5762913), type 1 diabetic children (ID: 71031655), and peripheral blood CD4 T cells of lupus erythematosus patients (ID: 95270555). (G-H) Immunohistochemistry for PD-1 expression in tissues of colon and skin of mice (n=3). Scale bar 50 μm. (I-J) Representative quantification of PD-1 in colon, and skin tissues analyzed by flow cytometry (n=3). (K-L) mRNA level of PD-1 in colon and skin tissues measured by qPCR (n=3). Data are represented as mean ± SEM. Statistical significance was calculated by Student's *t*-test. **P*<0.05, ***P*<0.01, ****P*<0.001.

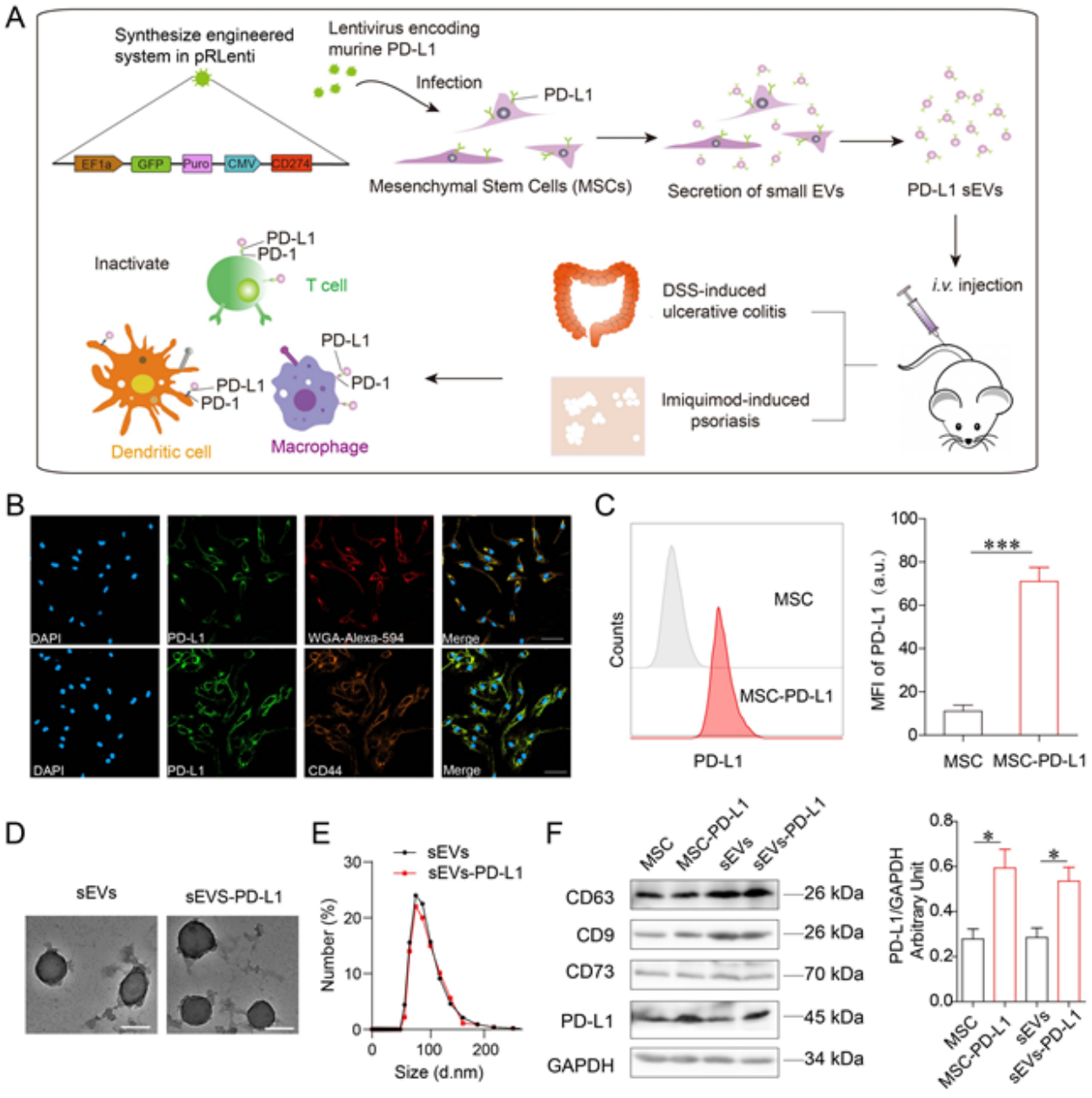

Fig. 2. Schematic and characterization of MSC-sEVs-PD-L1. (A) Schematic illustration of the establishment of mesenchymal stem cell derived small extracellular vesicles (MSC-sEVs) with PD-L1 overexpression and inhibition of activated T cells, macrophages and DCs for immune diseases alleviation. (B). GFP-PD-L1 expression (green) and co-localization with cell membrane dye Alexa Fluor 594-conjugated wheat germ agglutinin (red) (WGA594) and MSC marker CD44 (orange) was detected by immunofluorescence after infected with lentivirus. Scale bar 50 μm. (C) PD-L1 expression on MSCs was analyzed by flow cytometry (left).

Representative quantification of mean fluorescence intensity (MFI) of PD-L1 (n=3) (right). (D) Representative transmission electron microscope (TEM) images of MSC-sEVs and MSC-sEVs-PD-L1, scale bar, 100 nm. (E) Size distribution of MSC-sEVs and MSC-sEVs-PD-L1 by dynamic light scattering (DLS). (F) Extracellular vesicles marker of CD63, CD9, CD73 and PD-L1 expression on MSC-sEVs was detected by Western blot (left). Relative value of PD-L1/GAPDH stripe gray (right) (n=3). Data are represented as mean ± SEM. Statistical significance was calculated by Student's *t*-test. **P*<0.05, ****P*<0.001.

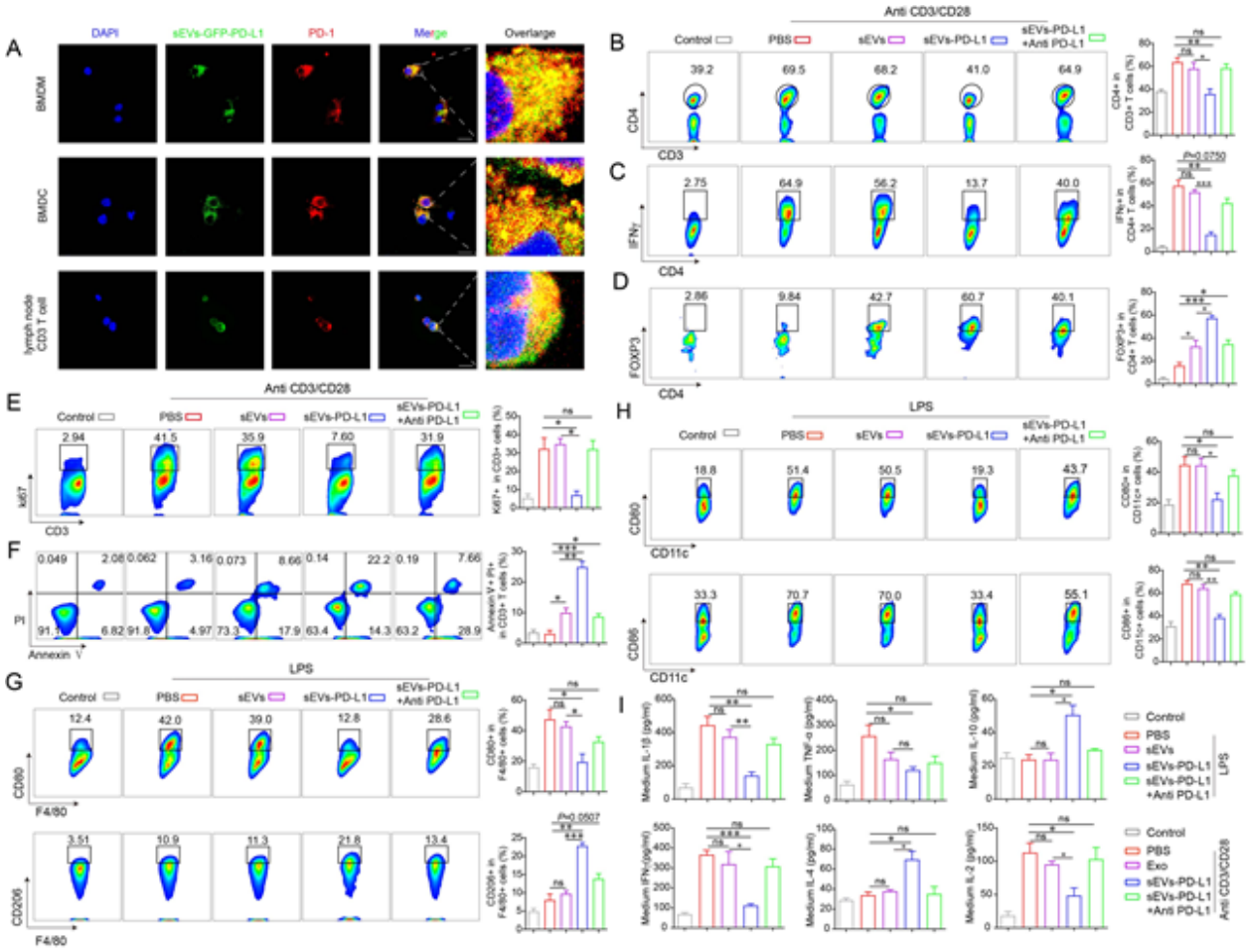

Fig. 3. MSC-sEVs-PD-L1 interacted with PD-1 and effectively inhibited immune cells activation *in vitro*. (A) Co-localization of sEVs-GFP-PD-L1 (green) and PD-1 (red) on activated BMDM cells, BMDC and lymph node T cells was displayed by immunofluorescence staining. The nuclei were stained with DAPI. Scale bar, 5 μm. Representative plots (left) and quantification (right) of lymph node CD4+ CD3+ T cells (B), lymph node IFN-γ+ CD4+ T cells (C), lymph node Foxp3+ CD4+ T cells (D), lymph node Ki67+ CD3+ T cells (E), lymph node Annexin V+ / PI+ CD3+ T cells (F), CD80+, CD206+ BMDM cells (G), and BMDCs CD80+, CD86+ in CD11c+ cells (H) in different treatment groups analyzed by flow cytometry. (I) Cytokines in medium released from BMDM cells and lymphocytes in different treatment groups were measured by Elisa kits. Data are represented as mean ± SEM of three independent experiment. Statistical significance was calculated by Student's *t*-test. **P*<0.05, ***P*<0.01, ****P*<0.001, ns, non-significant.

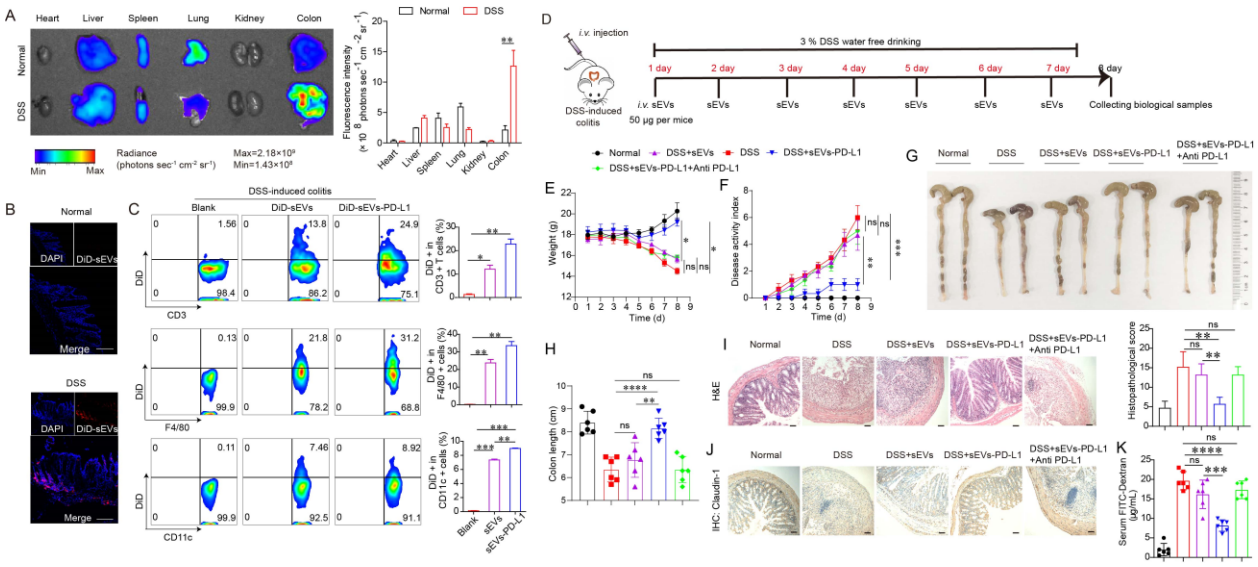

Fig. 4. MSC-sEVs-PD-L1 ameliorated DSS-induced ulcerative colitis. (A) DiD-labelled MSC-sEVs-PD-L1 were injected through the tail-vein in mice for 24 h. *In vivo* fluorescence images of MSC-sEVs-PD-L1 in major organs (left). Fluorescence intensity per gram of tissue in major organs (right) (n=3). (B) DiD-labelled MSC-sEVs-PD-L1 accumulation in colon tissue analyzed by immunofluorescence. (C) Representative plots (left) and quantification (right) of DiD-labelled sEVs-PD-L1 interacting with CD3+ T cells, F4/80+ cells and CD11c+ cells analyzed by flow cytometry (n=3). (D) Schematic representation of DSS-induced mouse ulcerative colitis and MSC-sEVs, MSC-sEVs-PD-L1, MSC-sEVs-PD-L1+Anti PD-L1 treatment. (E) Loss of basal body weight of each group during the disease process (n=6). (F) Disease activity index (DAI) was calculated (n=6). (G) Macroscopic appearance and (H) the length of colons from each group of mice were measured (n=6). (I) Paraffin-embedded colon sections were stained with H&E for light microscopy assessment. Scale bar 50 μm. Histopathological score were assessed for disease severity (right) (n=6). (J) Tight junction protein level of Claudin-1 in colon tissue sections was measured by immunohistochemical staining (n=3). Scale bar 50 μm. (K) Serum concentration of FITC dextran were measured 4 h after oral administration to mice on day 7 (n=6). Data are represented as mean ± SEM. Statistical significance was calculated by Student's *t*-test. **P*<0.05, ***P*<0.01, ****P*<0.001, *****P*<0.0001, ns, non-significant.

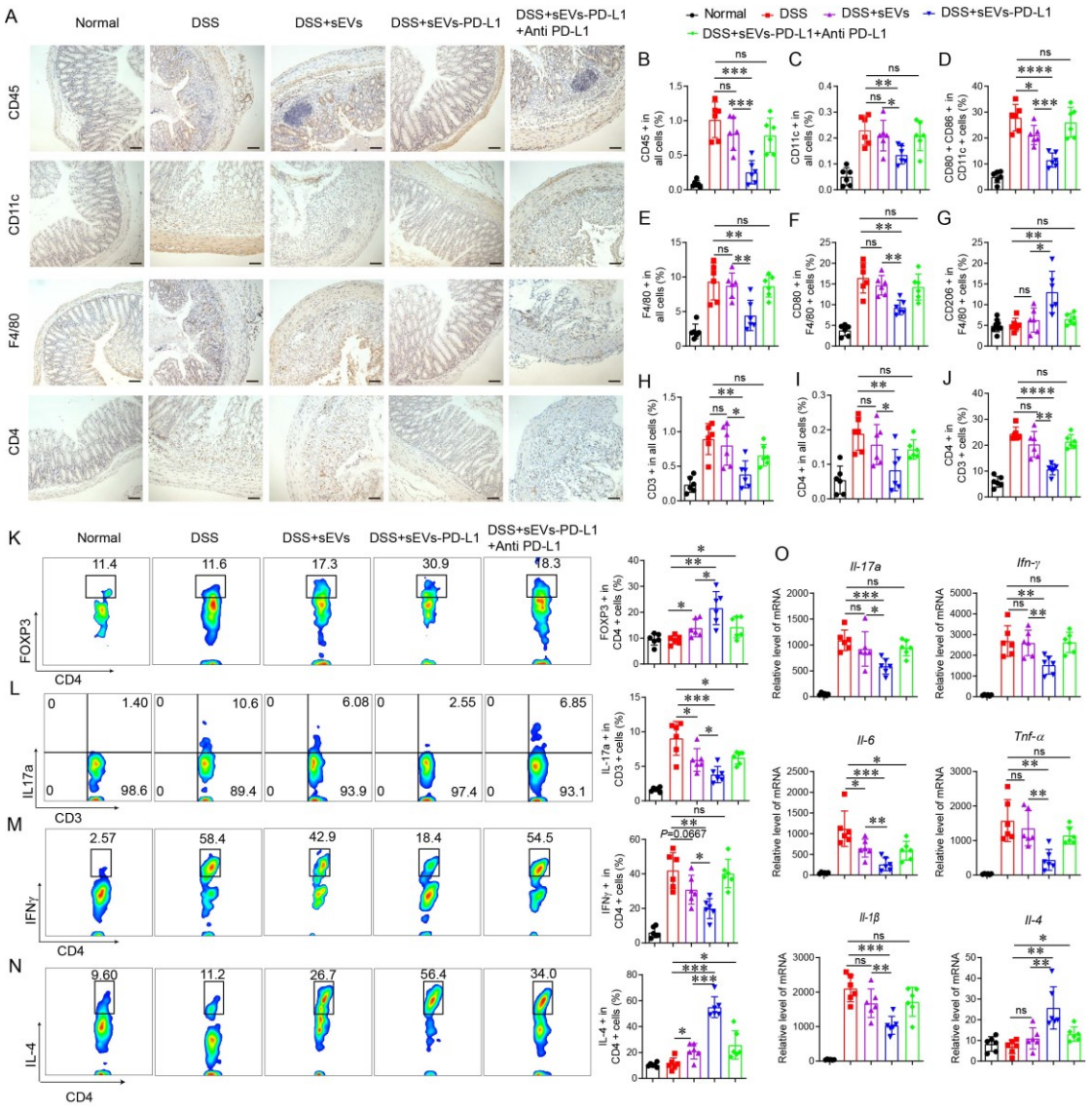

Fig. 5. MSC-sEVs-PD-L1 reshaped the inflammatory ecosystem in colon of colitis mice. (A) Infiltration of CD45, CD11c, F4/80 and CD4 in colon tissue sections from each group of mice was measured by immunohistochemical staining (n=3). Scale bar 50 μm. (B-J) Representative quantification of CD45+, CD11c+, CD80+ CD86+ CD11c+, F4/80+, CD80+ F4/80+, CD206+ F4/80+, CD3+, CD4+, CD4+ CD3+ cells in colon tissues of different treatment groups analyzed by flow cytometry (n=6). (K-N) Representative plots (left) and quantification (right) of Foxp3+ CD4+, IL-17a+CD3+, IFN-γ+CD4+ and IL-4+CD4+ cells in colon tissues of different treatment groups analyzed by flow cytometry (n=6). (O) mRNA relative levels of *Il-17a*, *Ifn-γ*, *Il-6*, *Tnf-α*, *Il-1β* and *Il-4* in colon tissues of different treatment groups measured by qPCR (n=6). Data are represented as mean ± SEM. Statistical significance was calculated by Student's *t*-test. **P*<0.05, ***P*<0.01, ****P*<0.001, *****P*<0.0001, ns, non-significant. .

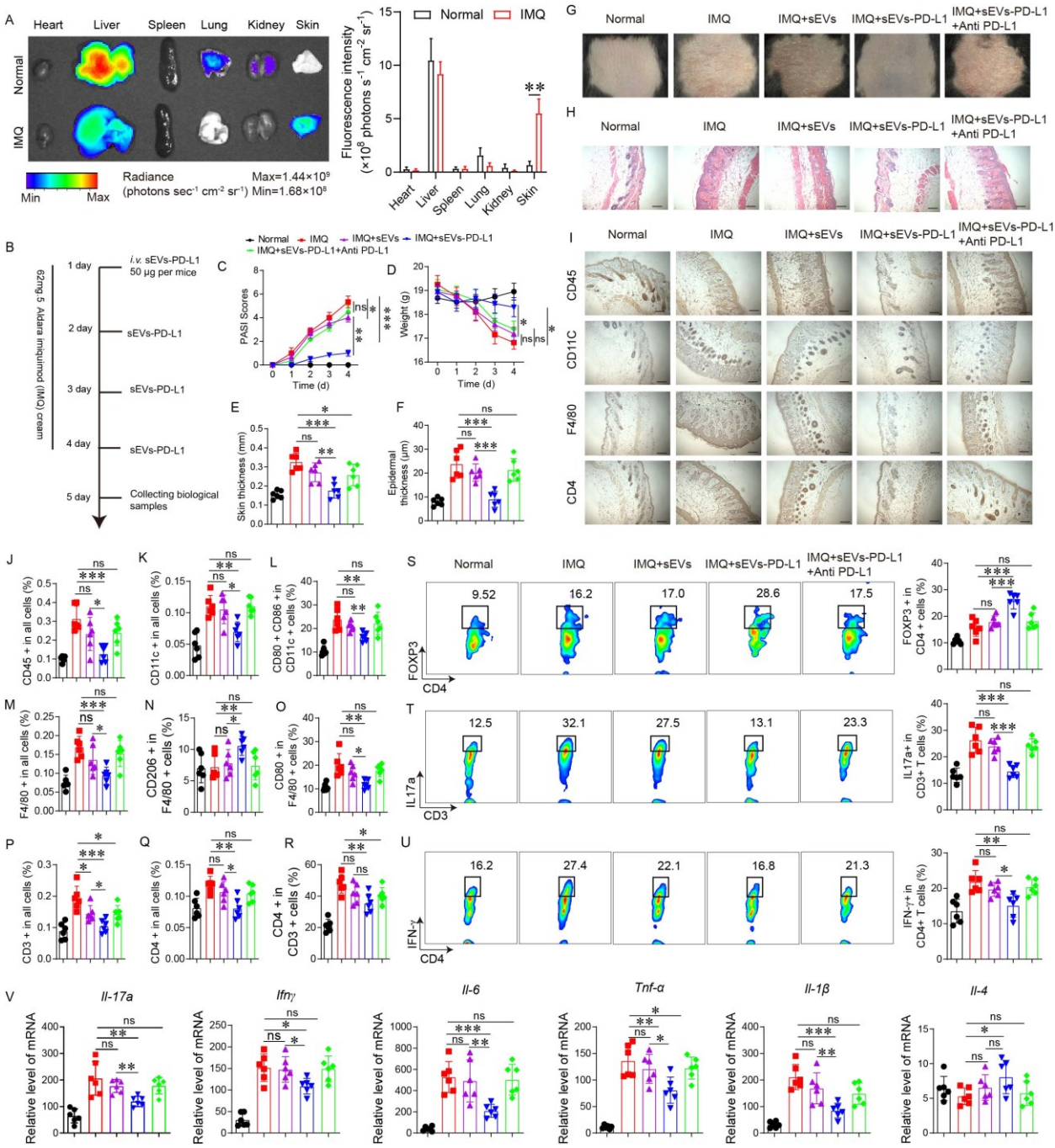

Fig. 6. MSC-sEVs-PD-L1 ameliorated IMQ-induced psoriasis. (A) DiD-labelled MSC-sEVs-PD-L1 were injected through the tail-vein in mice for 12 h. *In vivo* fluorescence images of MSC-sEVs-PD-L1 in major organs (left). Fluorescence intensity per gram of tissue in major organs (right) (n=3). (B) Schematic representation of IMQ-induced mouse psoriasis and MSC-sEVs, MSC-sEVs-PD-L1, MSC-sEVs-PD-L1+Anti PD-L1 treatment. (C) Clinical scores and (D) weight in each group were monitored (n=6). (E) Skin thickness and (F)

epidermal thickness were measured (n=6). (G) Photograph of mice back skin taken on day 4. (H) Paraffin-embedded skin sections were stained with H&E for light microscopy assessment (n=3). Scale bar 50 μm. (I) Infiltration of CD45, CD11c, F4/80 and CD4 in skin tissue sections was measured by immunohistochemical staining (n=3). Scale bar 50 μm. (J-S) Representative quantification of CD45+, CD11c+, CD80+ CD86+ CD11c+, F4/80+, CD80+ F4/80+, CD206+ F4/80+, CD3+, CD4+, CD4+ CD3+, Foxp3+ CD4+ cells in skin tissues of different treatment groups analyzed by flow cytometry (n=6). (T-U) Representative plots (left) and quantification (right) of IL-17a+CD3+ and IFN-γ+CD4+ T cells in skin tissues of different treatment groups analyzed by flow cytometry (n=6). (V) mRNA relative levels of *Il-17a*, *Ifn-γ*, *Il-6*, *Tnf-α*, *Il-1β* and *Il-4* in skin tissues of different treatment groups measured by qPCR (n=6). Data are represented as mean ± SEM. Statistical significance was calculated by Student's *t*-test. **P*<0.05, ***P*<0.01, ****P*<0.001, ns, non-significant.

.

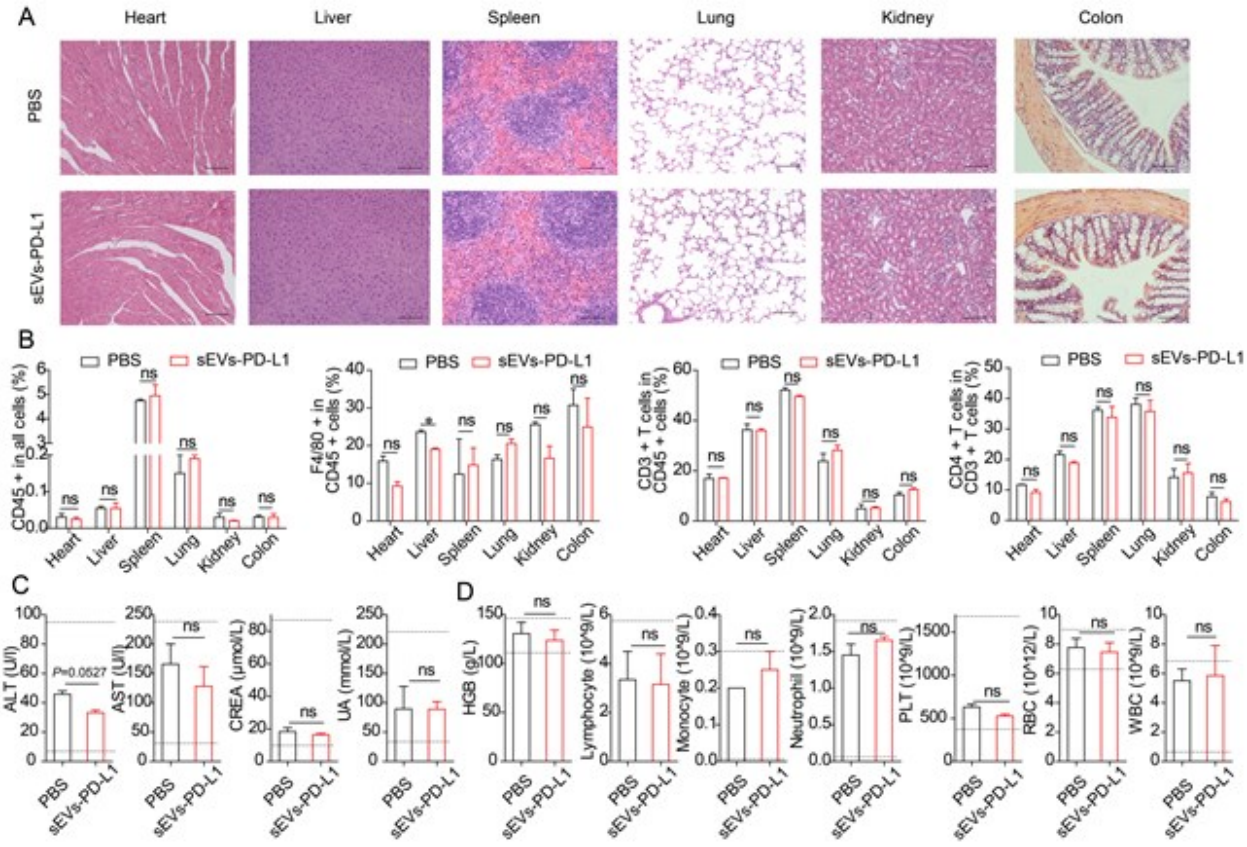

Fig. 7. Safety evaluation of MSC-sEVs-PD-L1 *in vivo*. (A) Paraffin-embedded tissue sections were stained with H&E for light microscopy assessment (n=3). Scale bar 50 μm. (B) Representative quantification of CD45+ cells, F4/80+ CD45+ cells, CD3+ CD45+ cells, CD4+ CD3+ cells in major tissue treated with or without MSC-sEVs-PD-L1 analyzed by flow cytometry (n=3). (C) ALT, AST, CREA, UA was measure by blood biochemical examination (n=3). Normal value range is within two dotted lines. (D) Blood routine examination (n=3). Normal value range is within two dotted lines. Data are represented as mean ± SEM. Statistical significance was calculated by Student's *t*-test. **P*<0.05, ns, non-significant.

Referance

[1] L. C. Rankin, D. Artis, *Cell* **2018**, *173*, 554.

[2] S. P. Weisberg, B. B. Ural, D. L. Farber, *Cell* **2021**, *184*, 1517.

[3] L. Fugger, L. T. Jensen, J. Rossjohn, *Cell* **2020**, *181*, 63.

[4] J. Varade, S. Magadan, A. Gonzalez-Fernandez, *Cell Mol Immunol* **2021**, *18*, 805.

[5] W. E. Ruff, T. M. Greiling, M. A. Kriegel, *Nat Rev Microbiol* **2020**, *18*, 521.

[6] K. M. Kingsmore, A. C. Grammer, P. E. Lipsky, *Nat Rev Rheumatol* **2020**, *16*, 32.

[7] D. M. Schwartz, Y. Kanno, A. Villarino, M. Ward, M. Gadina, J. J. O'Shea, *Nat Rev Drug Discov* **2017**, *16*, 843.

[8] N. M. Edner, G. Carlesso, J. S. Rush, L. S. K. Walker, *Nat Rev Drug Discov* **2020**, *19*, 860.

[9] S. Kang, T. Tanaka, M. Narazaki, T. Kishimoto, *Immunity* **2019**, *50*, 1007.

[10] A. A. Zarrin, K. Bao, P. Lupardus, D. Vucic, *Nat Rev Drug Discov* **2021**, *20*, 39.

[13] A. Cifuentes-Rius, A. Desai, D. Yuen, A. P. R. Johnston, N. H. Voelcker, *Nat Nanotechnol* **2021**, *16*, 37.

[12] M. N. Wykes, S. R. Lewin, *Nat Rev Immunol* **2018**, *18*, 91.

[13] C. Sun, R. Mezzadra, T. N. Schumacher, *Immunity* **2018**, *48*, 434.

[14] J. Wang, T. Yoshida, F. Nakaki, H. Hiai, T. Okazaki, T. Honjo, *Proc Natl Acad Sci U S A* **2005**, *102*, 11823.

[15] H. Nishimura, M. Nose, H. Hiai, N. Minato, T. Honjo, *Immunity* **1999**, *11*, 141.

[16] Z. Wang, C. A. Huang, *Nat Biomed Eng* **2019**, *3*, 253.

[17] D. Sugiura, T. Maruhashi, I. M. Okazaki, K. Shimizu, T. K. Maeda, T. Takemoto, T. Okazaki, *Science* **2019**, *364*, 558.

[18] F. Martins, L. Sofiya, G. P. Sykiotis, F. Lamine, M. Maillard, M. Fraga, K. Shabafrouz, C. Ribi, A. Cairoli, Y. Guex-Crosier, T. Kuntzer, O. Michielin, S. Peters, G. Coukos, F. Spertini, J. A. Thompson, M. Obeid, *Nat Rev Clin Oncol* **2019**, *16*, 563.

[19] A. Simonaggio, J. M. Michot, A. L. Voisin, J. Le Pavec, M. Collins, A. Lallart, G. Cengizalp, A. Vozy, A. Laparra, A. Varga, A. Hollebecque, S. Champiat, A. Marabelle, C. Massard, O. Lambotte, *JAMA Oncol* **2019**, *5*, 1310.

[20] V. Koliaraki, A. Prados, M. Armaka, G. Kollias, *Nat Immunol* **2020**, *21*, 974.

[21] J. Galipeau, L. Sensebe, *Cell Stem Cell* **2018**, *22*, 824.

[22] S. Fujii, Y. Miura, A. Fujishiro, T. Shindo, Y. Shimazu, H. Hirai, H. Tahara, A. Takaori-Kondo, T. Ichinohe, T. Maekawa, *Stem Cells* **2018**, *36*, 434.

[23] L. P. Andrews, H. Yano, D. A. A. Vignali, *Nat Immunol* **2019**, *20*, 1425.

[24] M. A. Gholampour, S. Abroun, R. Nieuwland, S. J. Mowla, S. Soudi, *J Cell Physiol* **2021**, *236*, 6055.

[25] T. Kobayashi, B. Siegmund, C. Le Berre, S. C. Wei, M. Ferrante, B. Shen, C. N. Bernstein, S. Danese, L. Peyrin-Biroulet, T. Hibi, *Nat Rev Dis Primers* **2020**, *6*, 74.

[26] C. E. M. Griffiths, A. W. Armstrong, J. E. Gudjonsson, J. Barker, *Lancet* **2021**, *397*, 1301.

[27] D. B. Doroshow, S. Bhalla, M. B. Beasley, L. M. Sholl, K. M. Kerr, S. Gnjatic, Wistuba, II, D. L. Rimm, M. S. Tsao, F. R. Hirsch, *Nat Rev Clin Oncol* **2021**, *18*, 345.

[28] X. Zhang, Y. Kang, J. Wang, J. Yan, Q. Chen, H. Cheng, P. Huang, Z. Gu, *Adv Mater* **2020**, *32*, e1907692.

[29] L. C. Davies, N. Heldring, N. Kadri, K. Le Blanc, *Stem Cells* **2017**, *35*, 766.

[30] S. Mardpour, S. N. Hassani, S. Mardpour, F. Sayahpour, M. Vosough, J. Ai, N. Aghdami, A. A. Hamidieh, H. Baharvand, *J Cell Physiol* **2018**, *233*, 9330.

[31] Z. Liao, S. Li, S. Lu, H. Liu, G. Li, L. Ma, R. Luo, W. Ke, B. Wang, Q. Xiang, Y. Song, X. Feng, Y. Zhang, X. Wu, W. Hua, C. Yang, *Biomaterials* **2021**, *274*, 120850.

[32] Y. Sun, H. Shi, S. Yin, C. Ji, X. Zhang, B. Zhang, P. Wu, Y. Shi, F. Mao, Y. Yan, W. Xu, H. Qian, *ACS Nano* **2018**, *12*, 7613.

[33] K. Andreas, M. Sittinger, J. Ringe, *Trends Biotechnol* **2014**, *32*, 483.

[34] Y. J. Liu, D. D. Sun, Q. Fan, Q. L. Ma, Z. L. Dong, W. W. Tao, H. Q. Tao, Z. Liu, C. Wang, *Nano Res* **2020**, *13*, 564.

[35] T. Koutsokeras, T. Healy, *Nat Rev Drug Discov* **2014**, *13*, 173.

[36]M. T. Patrick, P. E. Stuart, K. Raja, J. E. Gudjonsson, T. Tejasvi, J. Yang, V. Chandran, S. Das, K. Callis-Duffin, E. Ellinghaus, C. Enerback, T. Esko, A. Franke, H. M. Kang, G. G. Krueger, H. W. Lim, P. Rahman, C. F. Rosen, S. Weidinger, M. Weichenthal, X. Wen, J. J. Voorhees, G. R. Abecasis, D. D. Gladman, R. P. Nair, J. T. Elder, L. C. Tsoi, *Nat Commun* **2018**, *9*, 4178.

[37]M. B. Geuking, R. Burkhard, *Mucosal Immunol* **2020**, *13*, 855.

[38]H. Park, S. Lad, K. Boland, K. Johnson, N. Readio, G. Jin, S. Asfaha, K. S. Patterson, A. Singh, X. Yang, D. Londono, A. Singh, C. Trempus, D. Gordon, T. C. Wang, R. J. Morris, *Nat Commun* **2018**, *9*, 5293.

[39]J. Yan, Q. Zhao, K. Gabrusiewicz, L. Y. Kong, X. Xia, J. Wang, M. Ott, J. Xu, R. E. Davis, L. Huo, G. Rao, S. C. Sun, S. S. Watowich, A. B. Heimberger, S. Li, *Nat Commun* **2019**, *10*, 448.

[40]H. Nasser, P. Adhikary, A. Abdel-Daim, O. Noyori, J. Panaampon, R. Kariya, S. Okada, W. Ma, M. Baba, H. Takizawa, M. Yamane, H. Niwa, S. Suzu, *Cell Death Discov* **2020**, *6*, 63.

[41]S. Shen, H. Dai, Z. Fei, Y. Chai, Y. Hao, Q. Fan, Z. Dong, Y. Zhu, J. Xu, Q. Ma, X. Han, L. Xu, F. Peng, Z. Liu, C. Wang, *ACS Nano* **2021**, *15*, 9111.

[42]M. Soleimani, S. Nadri, *Nat Protoc* **2009**, *4*, 102.

[43]G. R. Willis, A. Fernandez-Gonzalez, M. Reis, V. Yeung, X. Liu, M. Ericsson, N. A. Andrews, S. A. Mitsialis, S. Kourembanas, *J Extracell Vesicles* **2020**, *9*, 1790874.

[44]B. Liu, B. Ye, X. Zhu, L. Yang, H. Li, N. Liu, P. Zhu, T. Lu, L. He, Y. Tian, Z. Fan, *Nat Commun* **2020**, *11*, 4076.

[45]M. M. Ning, W. J. Yang, W. B. Guan, Y. P. Gu, Y. Feng, Y. Leng, *Acta Pharmacol Sin* **2020**, *41*, 1446.

[46]H. Alrefai, K. Muhammad, R. Rudolf, D. A. Pham, S. Klein-Hessling, A. K. Patra, A. Avots, V. Bukur, U. Sahin, S. Tenzer, M. Goebeler, A. Kerstan, E. Serfling, *Nat Commun* **2016**, *7*, 11724.

[47]L. Feng, P. Song, F. Xu, L. Xu, F. Shao, M. Guo, W. Huang, L. Kong, X. Wu, Q. Xu, *J Invest Dermatol* **2019**, *139*, 1946.

[48]X. Zhang, F. Xu, L. Liu, L. Feng, X. Wu, Y. Shen, Y. Sun, X. Wu, Q. Xu, *Int Immunopharmacol* **2017**, *53*, 1.

[49] Y. Lee, K. Sugihara, M. G. Gillilland, 3rd, S. Jon, N. Kamada, J. J. Moon, *Nat Mater* **2020**, *19*, 118.

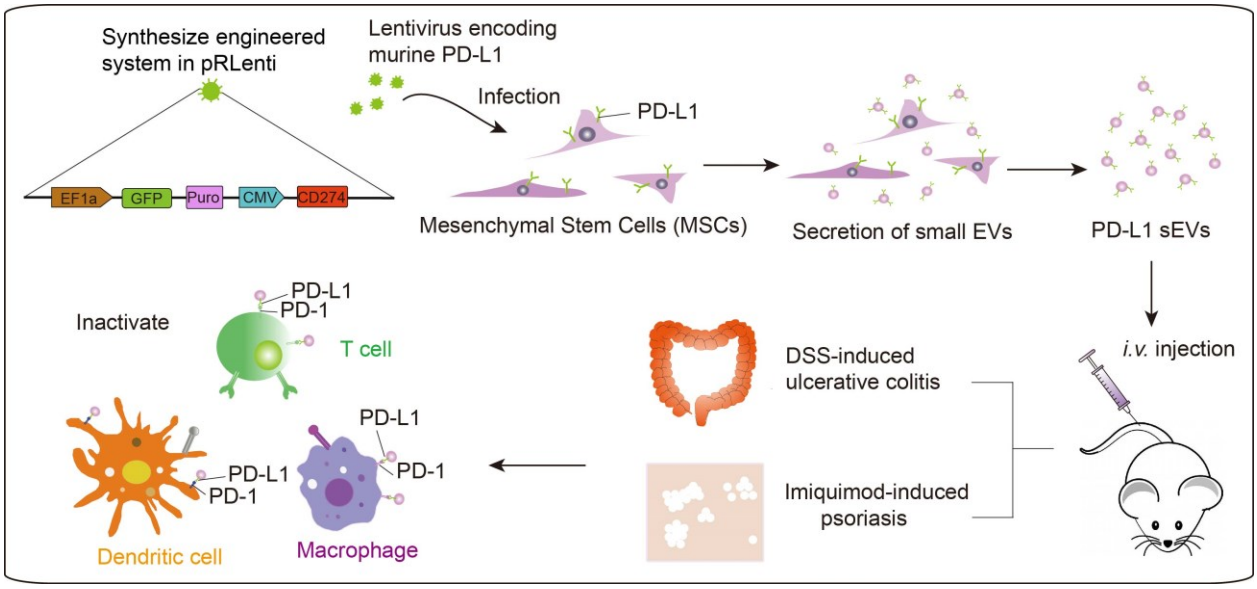

High-expressing PD-L1 extracellular vesicles derived from mesenchymal stem cells are prepared for autoimmune diseases treatment. As cell-free carrier, MSC-sEVs-PD-L1 restore tissue lesion by reshaping the local immune microenvironment via PD-1/PD-L1 pathway, which might potentially provide a universal platform technique for the immunotherapy of various autoimmune diseases.